

High Range Resolution Synthesized by Non-linear Stepped-Frequency Chirp Pulse Train

Yingrui Hu and Xuegang Wang

Department of Electronics Engineering

University of Electronic Science and Technology of China
No.4, Sec.2, Jianshe North Road, Chengdu Sichuan, 610054
P.R.China

raymond706@hotmail.com and xgwang@ee.uestc.edu.cn

Abstract: - Traditional stepped frequency chirp pulse train methods suffer from high sidelobes and ambiguous peaks, known as grating lobes and difficulty in compensating Doppler effect caused by target motion. This paper investigates a class of non-linear stepped frequency chirp pulse train with low sidelobes and capability to cancel clutter and to compensate motion. We present analytic expression for its autocorrelation function (ACF) and propose an improved method to produce the non-linear stepped frequency chirp pulse train with small grating lobes and small overlap ratio for sub-pulse of large time bandwidth product. A method for estimation a target's radial velocity is developed, which avoids multiple bursts required by other methods. The high signal-to-noise (SNR) ratio as a result of sub-pulse compression assures the accuracy of estimation. The Cramer-Rao bound for lower limit on the velocity estimation of the pulse train is derived to demonstrate its performance.

Key-Words: Non-linear stepped-frequency chirp pulse train, Autocorrelation function, Grating lobes suppression, Motion compensation, Cramer-Rao bound, One-dimensional range profile

1 Introduction

Radars commonly use wide bandwidth pulses to attain high range resolution [1]. However when such wideband pulses are unavailable, high range resolution can still be achieved by coherently combining a sequence of narrowband pulses spanning the desired bandwidth [2]. This technique is known as stepped-frequency pulse train. The main advantage of such approach is that it achieves the large synthetic wideband while maintaining relatively small instantaneous system bandwidth.

But this approach suffers from high sidelobes and grating lobes in the range response. Conventional technology uses heavy spectral weighting and highly overlapped pulses to control them with the cost of SNR loss and other undesirable attributes. Another unfortunate drawback of this approach is that target energy spills over into consecutive coarse range bins due to the matched-filter operation. This is the main reason why it is not regarded as a suitable method to process SAR images [3]. In addition, radar detection distance of the stepped-frequency pulse train is limited under the precondition of the definite range resolution. By substituting the conventional narrowband sub-pulses with chirp sub-pulses, high

range resolution can be realized and the detection distance can also be increased accordingly [4]. Additional advantage of replacing the fix-frequency pulse with chirp pulses is help to lower the grating lobes that appear in the range response.

The stepped-frequency pulse train is also sensitive to target motion. The Doppler effect introduces phase distortion and causes range cell shift, power spreading and false peaks in the range profile [5]. Motion compensation is necessary for this approach to obtain a reasonable one-dimensional range profile.

In this paper we investigate a class of non-linear stepped-frequency chirp pulse train modified from conventional stepped-frequency chirp pulse train with low sidelobes and capability to cancel clutter and to compensate target motion.

The non-linear stepped-frequency chirp pulse train we consider here consists of N steps with initial transmitted frequency f_0 , frequency step size Δf . Each sub-pulse is chirp waveform with bandwidth B , duration T_p , pulse repetition interval T_r and frequency modulation slope $K = B/T_p$. All of these parameters are constant. The total signal bandwidth is $B_N = N\Delta f$. The center

frequency of the i^{th} step frequency is $f_i = f_0 + i\Delta f$, where $0 \leq i \leq N - 1$. We assume a positive frequency modulation slope here ($K > 0$), but the results apply to a negative slope as well.

We analyse the grating lobes of the non-linear stepped-frequency chirp pulse train and suggest a modified approach to suppress them. It can be considered as an improvement of method introduced in [6], which allows us to widen the range of parameters selection and find waveforms with large $T_p B$, small overlap ratio $B/\Delta f$ and small grating lobes. It is easy to realize in a practical system.

We also propose a new method to estimate the target radial velocity in one burst. The accuracy of estimation is assured by high SNR as a result of sub-pulse compression. The Cramer-Rao bound for lower limit on the velocity estimation of the pulse train is derived to verify its performance.

2 Non-Linear Stepped-Frequency Chirp Pulse Train

In non-linear stepped-frequency chirp pulse train, the aggregate burst distributes energy across the desired band in a non-uniform fashion way. The non-linearity could be implemented by transmitting different number of repetitions on each frequency carrier [7]. In essence, more pulses are used near the center of the desired band and fewer pulses are used near the edges. By coherently integrating the pulses of the same frequency carrier, it will distribute energy in a way that approximates a desired spectral weighting. Through so, we could achieve a reduction in range sidelobes akin to that achieved by a similar spectral weighting function used on receive. However, since this weighting is done on transmit, we avoid the SNR loss associated with the traditional receive-weighting technology. So it will provide higher SNR of one-dimensional range profile and longer detection range. By adjusting the repetition number on each frequency carrier, it will distribute the energy similar to any spectral weighting function according to practical requirement and reach practically any desired sidelobes level. The transmitted signal of the non-linear stepped-frequency chirp pulse train can be written as:

$$s(t) = \frac{1}{\sqrt{lT_p}} \sum_{i=0}^{N-1} \sum_{m=q_i}^{q_i-1} \text{rect}\left(\frac{t - mT_r}{T_p}\right) \cdot \exp[j\pi K(t - mT_r)^2] \exp[j2\pi(f_0 + i\Delta f)t] \quad (1)$$

where $\text{rect}\left(\frac{t}{T}\right) \cdot \exp(j\pi Kt^2)$ is a chirp sub-pulse, $\text{rect}(\cdot)$ represents rectangular function.

Define the repetition number on each frequency carrier by vector $X = [b_0, b_1, \dots, b_{N-1}]$, where $b_0 \leq b_1 \leq \dots \leq b_{N/2}$, $b_0 = b_{N-1}$, $b_1 = b_{N-2}, \dots$, and

$$q_i = \begin{cases} \sum_{p=0}^i b_p & i \geq 0 \\ 0 & \text{others} \end{cases} \quad \text{represents the coefficient of}$$

T_r delay of the m^{th} sub-pulse. The total number of sub-pulses transmitted is $l = \sum_{i=0}^{N-1} b_i$. Fig.1 shows its waveform and frequency law.

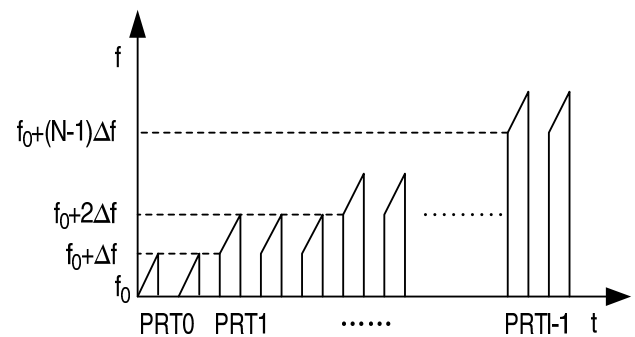


Fig.1a Waveform of non-linear stepped-frequency chirp pulse train

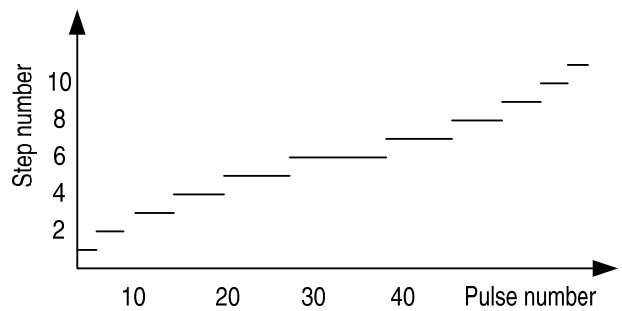


Fig.1b Frequency law of non-linear stepped-frequency chirp pulse train

3 ACF of the Non-linear Stepped-Frequency Chirp Pulse Train

Because of its non-linearity, we have to derive it according to the AF definition:

$$\begin{aligned} \chi(\tau, f_d) &= \int_{-\infty}^{+\infty} s(t)s^*(t+\tau)e^{j2\pi f_d t} dt \\ &= \frac{1}{lT_p} \sum_{i=0}^{N-1} \sum_{m=q_{i-1}}^{q_i-1} \sum_{h=0}^{N-1} \sum_{n=q_{h-1}}^{q_h-1} \int u(t-mT_r) \\ &\cdot u^*(t-nT_r+\tau) \exp[j2\pi(f_0+i\Delta f)t] \\ &\cdot \exp\{-j2\pi[f_0+h\Delta f](t+\tau)\} \exp(j2\pi f_d t) dt \end{aligned} \quad (2)$$

where $u(t) = \text{rect}(\frac{t}{T_p}) \cdot \exp(j\pi Kt^2)$

Applying replacement and reduction to Eq. (2), we can get:

$$\begin{aligned} \chi(\tau, f_d) &= \frac{1}{l} \sum_{i=0}^{N-1} \sum_{m=q_{i-1}}^{q_i-1} \sum_{h=0}^{N-1} \sum_{n=q_{h-1}}^{q_h-1} \exp[-j2\pi(f_0+h\Delta f)\tau] \\ &\cdot \exp\{j2\pi[f_d-(h-i)\Delta f]mT_r\} \\ &\cdot \chi_u[\tau-(n-m)T_r, f_d-(h-i)\Delta f] \end{aligned} \quad (3)$$

where χ_u is AF of chirp sub-pulse.

What we prefer is the center of AF, so we obtain:

$$\begin{aligned} \chi(\tau, f_d) &= \frac{1}{l} \sum_{i=0}^{N-1} \exp(j2\pi T_r f_d q_{i-1}) \cdot \frac{\sin(\pi T_r f_d b_i)}{\sin(\pi T_r f_d)} \\ &\cdot \exp[j(b_i-1)\pi T_r f_d] \cdot \exp(-j2\pi i\Delta f \tau) \cdot \chi_u(\tau, f_d) \end{aligned} \quad (4)$$

By setting $f_d = 0$, we yield magnitude of its time domain ACF for $|\tau| \leq T_p$:

$$|\chi(\tau, 0)| = \frac{1}{l} \cdot |\chi_u(\tau, 0)| \cdot \left| \sum_{i=0}^{N-1} b_i \cdot \exp(-j2\pi i\Delta f \tau) \right| \quad (5)$$

The ACF of the non-linear stepped-frequency chirp pulse train is relevant to repetition number on each frequency carrier. According to the symmetry of the weighting function simulated, we can decompose and integrate the Eq. (5).

$$|\chi(\tau, 0)| = \begin{cases} \frac{1}{l} \cdot |\chi_u(\tau, 0)| \cdot |\mathbf{x}_o \cdot \mathbf{h}_o| & N \text{ is odd} \\ \frac{1}{l} \cdot |\chi_u(\tau, 0)| \cdot |\mathbf{x}_e \cdot \mathbf{h}_e| & N \text{ is even} \end{cases} \quad (6)$$

where $\mathbf{x}_o = [b_0, b_1 - b_0, b_2 - b_1, \dots, 1]$, $\mathbf{x}_e = [b_0, b_1 - b_0, b_2 - b_1, \dots, 1, 1]$,

$$\begin{aligned} \mathbf{h}_o &= \left[\frac{\sin(N\pi\Delta f \tau)}{\sin(\pi\Delta f \tau)} \cdot \exp(j(N-1)\pi\Delta f \tau), \right. \\ &\frac{a_1 \cdot \sin((N-2)\pi\Delta f \tau)}{\sin(\pi\Delta f \tau)} \cdot \exp(j(N-3)\pi\Delta f \tau), \\ &\frac{a_2 \cdot \sin((N-4)\pi\Delta f \tau)}{\sin(\pi\Delta f \tau)} \cdot \exp(j(N-5)\pi\Delta f \tau), \\ &\left. \dots, \exp(-j2\pi \cdot \frac{N-1}{2} \cdot \Delta f \cdot \tau) \right]^T \end{aligned}$$

$$\begin{aligned} \mathbf{h}_e &= \left[\frac{\sin(N\pi\Delta f \tau)}{\sin(\pi\Delta f \tau)} \cdot \exp(j(N-1)\pi\Delta f \tau), \right. \\ &\frac{a_1 \cdot \sin((N-2)\pi\Delta f \tau)}{\sin(\pi\Delta f \tau)} \cdot \exp(j(N-3)\pi\Delta f \tau), \\ &\frac{a_2 \cdot \sin((N-4)\pi\Delta f \tau)}{\sin(\pi\Delta f \tau)} \cdot \exp(j(N-5)\pi\Delta f \tau), \\ &\left. \dots, \exp(-j2\pi \cdot \frac{N-2}{2} \Delta f \tau), \exp(-j2\pi \cdot \frac{N}{2} \Delta f \tau) \right]^T \\ a_i &= \exp(-j2\pi i\Delta f \tau). \end{aligned}$$

By setting $\tau = 0$, we yield magnitude of its frequency domain ACF:

$$\chi(0, f_d) = |\chi_u(0, f_d)| \cdot \left| \frac{\sin(\pi l T_r f_d)}{l \sin(\pi T_r f_d)} \right| \quad (7)$$

From Eq. (6) we find that the time domain ACF of the non-linear stepped-frequency pulse train is a kind of Sinc function. The range resolution is $1/N\Delta f$. According to Eq. (7), the Doppler resolution is $1/lT_r$. Compared to linear stepped-frequency train whose Doppler resolution is $1/NT_r$, the Doppler resolution of non-linear stepped-frequency pulse train is higher because l is much larger than N .

4 Grating Lobes Analysis and Suppression

Several methods to lower the range sidelobes and grating lobes of stepped-frequency pulse train were recently discussed. Reference [6] made use of the relationship between $T_p B$ and $T_p \Delta f$ to nullify several or even all grating lobes. But it resulted in large overlap ratio and large step number for wideband and limited parameters chosen in a great measure. Reference [2],[8],[9] were to use variable frequency steps according to a non-linear law such as chebyshev weighting function to mitigate sidelobes and reshape the spectrum resulting in a reduction of range sidelobes as well. But it still need inter-pulse weighting to lower these undesirable lobes. The method suggested in [10] presented enhanced processing schemes to compress signals with lower sidelobes and grating lobes. [11] had proposed genetic algorithms to eliminate grating lobes during scanning. Reference [12], [13] applied spatial variant apodization as non-linear windowing to lower down the lobes. Indeed, they are not only difficult to realize in practical system but also increase the orange of the system. Reference [14] suggested an extended correlation method to suppress the grating lobes. Reference [15] used

frequency MIMO technology to suppress the grating lobes. In [16], grating lobes were reduced by varying the pulse width, which destroyed the periodicity.

4.1 Grating Lobes Analysis

Clearly, according to Eq. (6), when $\tau = \frac{g}{\Delta f}$,

$|\mathbf{x} \cdot \mathbf{h}|$ reaches its maximum and the polynome also reaches its maximum value. So $|\chi(\tau,0)|$ exhibits peaks at

$$\tau_{lobe} = \frac{g}{\Delta f} \quad g = \pm 1, \pm 2, \dots \lfloor T_p \Delta f \rfloor \quad (8)$$

where $\lfloor x \rfloor$ implies the largest integer not exceeds x .

At these peaks, we find that the coefficient of polynome is positive when N is odd and N, g are even; the coefficient of polynome is negative when N is even and g is odd. So we can simplify the absolute value of Eq. (8).

$$|\chi(\tau,0)| = \begin{cases} \frac{1}{l} \cdot |\chi_u(\tau,0)| \cdot (\mathbf{x}_o \cdot \mathbf{h}_o) & N \text{ is odd} \\ \frac{1}{l} \cdot |\chi_u(\tau,0)| \cdot (\mathbf{x}_e \cdot \mathbf{h}_{ee}) & N \text{ and } g \text{ are even} \\ \frac{1}{l} \cdot |\chi_u(\tau,0)| \cdot (\mathbf{x}_e \cdot \mathbf{h}_{eo}) & N \text{ is even and } g \text{ is odd} \end{cases} \quad (9)$$

where

$$|\mathbf{h}_o| = \left[\left| \frac{\sin(N\pi\Delta f \tau)}{\sin(\pi\Delta f \tau)} \right|, \left| \frac{\sin[(N-2)\pi\Delta f \tau]}{\sin(\pi\Delta f \tau)} \right|, \left| \frac{\sin[(N-4)\pi\Delta f \tau]}{\sin(\pi\Delta f \tau)} \right|, \dots, 1 \right]^T$$

$$|\mathbf{h}_{ee}| = \left[\left| \frac{\sin(N\pi\Delta f \tau)}{\sin(\pi\Delta f \tau)} \right|, \left| \frac{\sin[(N-2)\pi\Delta f \tau]}{\sin(\pi\Delta f \tau)} \right|, \left| \frac{\sin[(N-4)\pi\Delta f \tau]}{\sin(\pi\Delta f \tau)} \right|, \dots, 1, 1 \right]^T$$

$$|\mathbf{h}_{eo}| = \left[\left| \frac{\sin(N\pi\Delta f \tau)}{\sin(\pi\Delta f \tau)} \right|, \left| \frac{\sin[(N-2)\pi\Delta f \tau]}{\sin(\pi\Delta f \tau)} \right|, \left| \frac{\sin[(N-4)\pi\Delta f \tau]}{\sin(\pi\Delta f \tau)} \right|, \dots, -1, -1 \right]^T$$

The time domain ACF of non-linear stepped-frequency chirp pulse train is can be written as:

$$|\chi(\tau,0)| = |R_1(\tau)| \cdot |R_2(\tau)| \quad |\tau| \leq T_p \quad (10)$$

where

$$|R_1(\tau)| = |\chi_u(\tau,0)| = \left| \left(1 - \frac{|\tau|}{T_p}\right) \text{sinc}\left[B\tau\left(1 - \frac{|\tau|}{T_p}\right)\right] \right| \quad \text{and}$$

$$|R_2(\tau)| = \frac{1}{l} \cdot |\mathbf{x} \cdot \mathbf{h}|.$$

$|R_2(\tau)|$ causes the appearance of the grating lobes and the grating lobes appear at the points of the maxim of $|R_2(\tau)|$. Fig.2 shows the two terms respectively. The simulation parameters are $N=16$, $f_0=10\text{GHz}$, $T_p\Delta f=120$, $T_pB=248$, $T_r=3T_p$, repetition number $X=[2, 3, 5, 8, 11, 13, 15, 16, 16, 15, 13, 11, 8, 5, 3, 2]$.

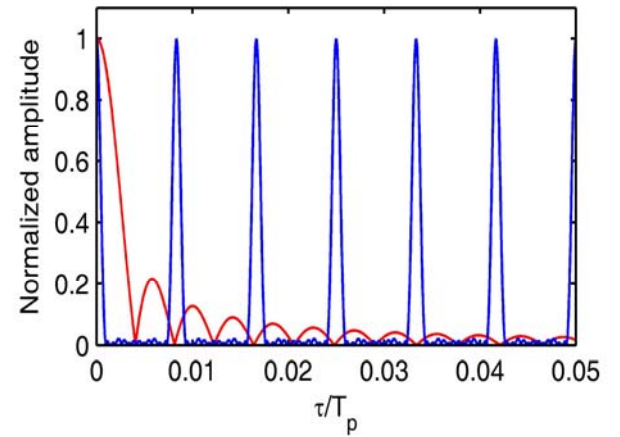


Fig.2 Grating lobes of non-linear stepped-frequency chirp pulse train. $|R_1(\tau)|$ (red line) and $|R_2(\tau)|$ (blue line)

4.2 Grating Lobes Suppression

Compared to conventional stepped-frequency chirp pulse train, the energy of smaller lobes between every two grating lobes is less and more energy lies on grating lobes. In order to nullify these grating lobes, we can let the nulls of $|R_1(\tau)|$ coincide with the peaks of $|R_2(\tau)|$, as [7] suggested. So we get:

$$T_p B = \frac{(au^2 - bv^2)^2}{uv(u-v)(au - bv)} \quad (11)$$

$$T_p \Delta f = \frac{au^2 - bv^2}{au - bv} \quad (12)$$

It forces that $|R_1(\tau)|$ exhibits its a^{th} and b^{th} ($b \geq a$) nulls exactly at the $|R_2(\tau)|$'s u^{th} and v^{th} ($v \geq u$) grating lobes. But it will result in large overlap ratio $B/\Delta f$ and large step number N for large $T_p B$ and

limit the parameters we can use for the most part. Also it may not take all grating lobes into account sometimes.

$$\frac{B}{\Delta f} = \frac{au^2 - bv^2}{uv(u - v)} \tag{13}$$

In fact, as long as the grating lobes level is less than some small value we can accepted, we achieve our goal. Specially

$$|R_l(\tau_{lobe})| \leq \delta \tag{14}$$

We denote δ as the grating lobe suppression factor. Applying Eq. (8) and Eq. (10) into (14)

$$\left| \sin\left[\pi B \frac{g}{\Delta f} \left(1 - \frac{g}{\Delta f t_p}\right)\right] \right| \leq \frac{\delta \pi B g}{\Delta f} \tag{15}$$

Thus by appropriately choosing the values of $B, T_p, \Delta f$ which satisfy the inequalities in Eq. (15) we can suppress the grating lobes of non-linear stepped frequency chirp pulse train to the desired δ level.

In these $\lfloor T_p \Delta f \rfloor$ inequalities, since the left hand side of Eq. (15) is no larger than 1, the inequalities with $g = g' + 1, g' = 2, \dots, \lfloor t_p \Delta f \rfloor$ already satisfy the Eq. (15), where $\frac{\delta \pi B g'}{\Delta f} = 1$. Fig.3 presents the plot of the smallest possible overlap $B / \Delta f$ as a function of $T_p \Delta f$ for $\delta = 0.025$ which produces grating lobes level $\leq -32dB$. It is the largest suppression level by improved parameter selection method.

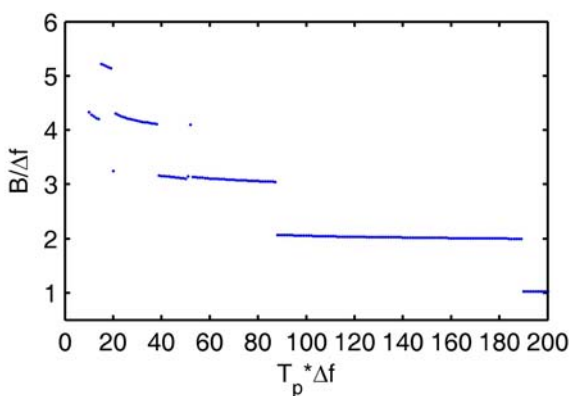


Fig.3 Smallest possible overlap $B / \Delta f$ for $T_p \Delta f$ when $\delta = 0.025$

From Fig.3 we know that it is possible to find the compromise parameters with relatively small overlap $B / \Delta f$ and small grating lobes for large

$T_p \Delta f$. And almost all grating lobes could be taken into account. Thus the approach to suppressing the grating lobes presented above allows us to widen the range of acceptable parameters significantly compared to [7]. The partial time domain ACF for three typical cases is shown in Fig.4.

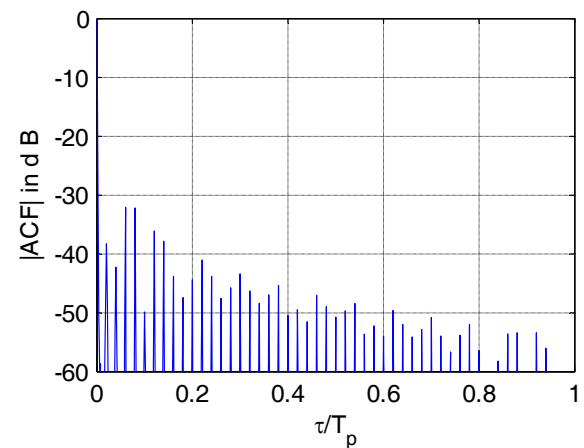
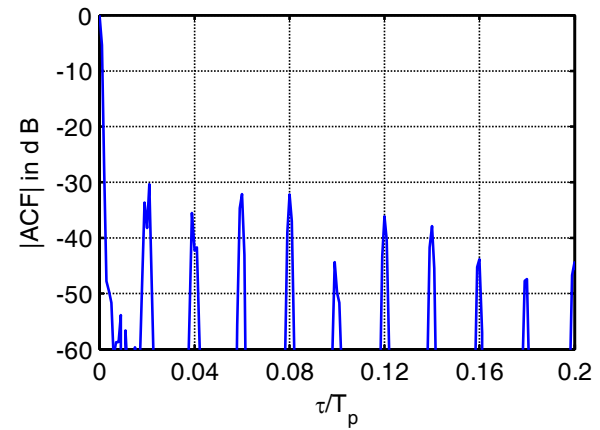
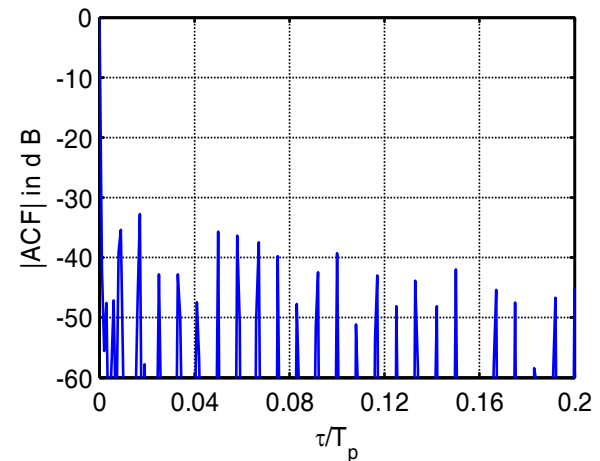


Fig.4a Partial ACF of typical case 1 $T_p \Delta f = 60, T_p B = 186, B / \Delta f = 3.1$



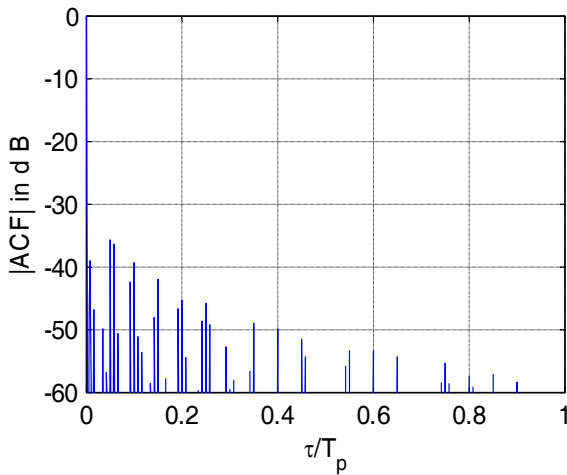


Fig.4b Partial ACF of typical case 2
 $T_p \Delta f = 120, T_p B = 248, B / \Delta f = 2.06$

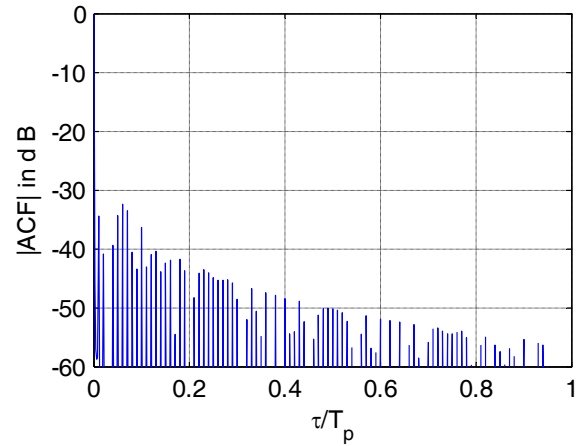
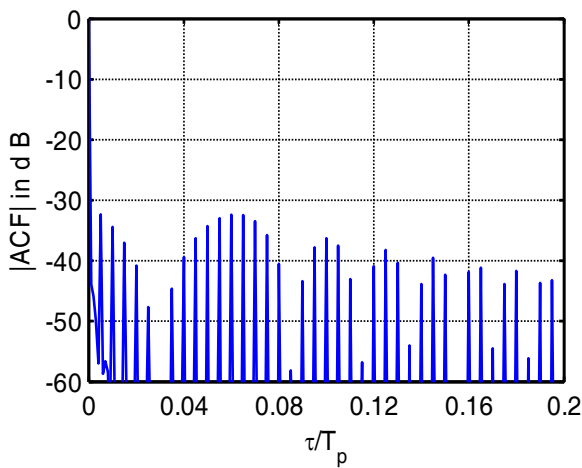


Fig.4c Partial ACF of typical case 3
 $T_p \Delta f = 200, T_p B = 206, B / \Delta f = 1.03$



It is evident from Fig.4 that the almost all the grating lobes are effectively suppressed at least 32dB. The small values are not only produced just at the τ_{lobe} themselves, but also around of the τ_{lobe} . For large $T_p \Delta f$, the overlap ratio is smaller. Fig.5 shows the AF of typical case 2.

From Fig.5 we can see that the grating lobe suppressing is effective for extended Doppler. The grating lobes build-up with Doppler is relatively slow. This behavior is typical of all the cases discussed here. Because of the overlap between pulses, there are relatively strong recurrent lobes volume in the recurrent lobes will be redistributed [7]. But the order of the pulses and step frequency repetition which simulates a similar spectral weighting do not alter the AF for $|\tau| \leq T_p$, so it

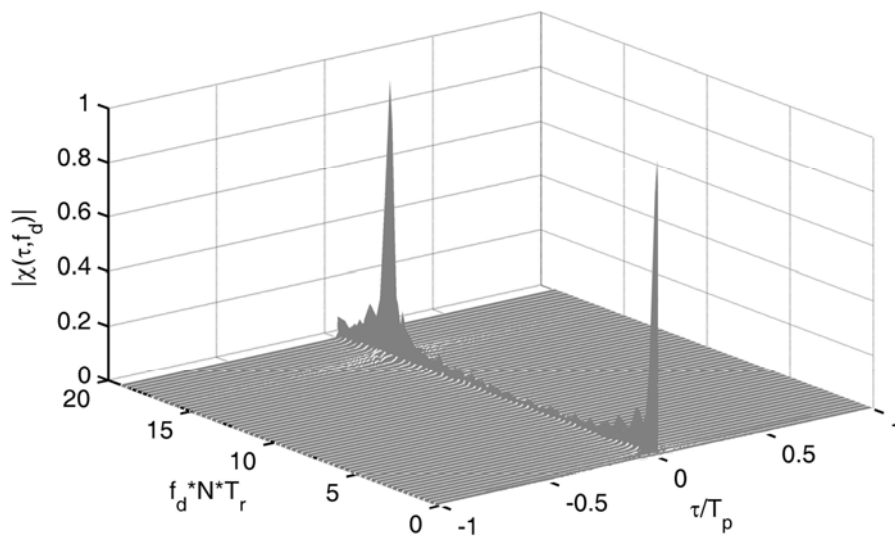


Fig.5 AF of typical case 2 $T_p \Delta f = 120, T_p B = 248, B / \Delta f = 2.06$

does not affect the suppressing procession.

5 Signal Processing of Non-linear Stepped-Frequency Chirp Pulse Train

First procession to its returns is coherent mixing and accomplishing the sub-pulse compression in each pulse repetition period. Denote that the target is R meters away from the radar and with the radial velocity v relative to the radar. The normalized mixing output of returns is:

$$y(t) = \sum_{i=0}^{N-1} \sum_{m=q_{i-1}}^{q_i-1} \text{rect}\left(\frac{t - mT_r - \tau}{T_p}\right) \cdot \exp[j\pi K(t - mT_r - \tau)^2] \exp[-j2\pi(f_0 + i\Delta f)\tau] \quad (16)$$

where $\tau = \frac{2}{c}(R - mT_r v - \frac{2R}{c}v)$.

The output of sub-pulse compression is:

$$y'(t) = \sum_{i=0}^{N-1} \sum_{m=q_{i-1}}^{q_i-1} \sqrt{KT_p^2} \text{rect}\left(\frac{t - mT_r - \tau}{T_p}\right) \cdot \frac{\sin[\pi KT_p(t - mT_r - \tau)]}{\pi KT_p(t - mT_r - \tau)} \exp[j\pi K(t - mT_r - \tau)^2] \cdot \exp(j\frac{\pi}{4}) \exp[-j2\pi(f_0 + i\Delta f)\tau] \quad (17)$$

From Eq. (17) we find that the phase of step frequency part is not affected by sub-pulse compression. Next step is the motion target indication (MTI) procession on each frequency carrier to cancel clutter. A similar method of the ground clutter cancellation with respect to the stepped frequency pulse train can be found in [17]. The specific analysis is presented in [4]. Then coherently integrate the pulses of the same frequency carrier by FFT, we will get maximum value point on each frequency carrier. The output is:

$$Y(k) = \sum_{i=0}^{N-1} \frac{\sin\{\pi[\frac{2vb_i T_r (f_0 + i\Delta f)}{c} - k_i]\}}{\sin\{\pi[\frac{2vT_r (f_0 + i\Delta f)}{c} - \frac{k_i}{b_i}]\}} \cdot \exp\{j\pi[\frac{2v(b_i - 1)T_r (f_0 + i\Delta f)}{c} - \frac{k_i(b_i - 1)}{b_i}]\} \cdot \exp[-j2\pi(f_0 + i\Delta f)\frac{2R}{c}] \quad (18)$$

The times of SNR improvement of each

coherent integration point is by factor b_i , the repetition number on each frequency carrier. So there will be different amplitude on each frequency carrier after integration because of the different number of pulses transmitted. Thus implements the approximate spectral weighting. Now the energy distribution over the band is similar to one of the weighting functions with SNR much higher than conventional weighting on receive, where signal spectrum is multiplied by normalized weighting function. The phase factor of step frequency part required to complement the IDFT on each frequency carrier is also contained. The Doppler effect caused by target motion introduces phase distortion and causes range cell shift, power spreading and false peaks in the range profile [5]. Motion compensation is necessary for this approach to obtain recognizable one-dimensional range profile. Lastly, IDFT is performed to these integration points to synthesize the high range resolution one-dimensional profile of the target. Fig.6 shows its coherent integration comparison to standard Chebyshev weighting. The simulation parameters are the same as typical case 2.

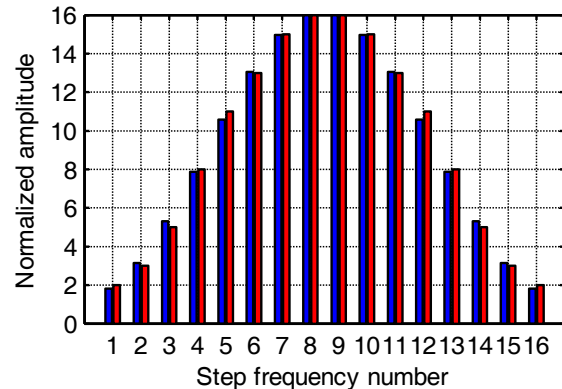


Fig.6 Coherent integration (right bars) comparison to theoretical Chebyshev weighting (left bars), ripple = 40dB

From Fig.6 we find that coherent integration implements the energy distribution over the band similar to theoretical Chebyshev weighting. It will achieve a reduction in range sidelobes akin to that achieved by a similar spectral weighting. Also it will partially suppress the grating lobes. But further method is needed to lower down the grating lobes. Fig.7 shows the range profile of a static point target 50 meters away in case 2. It is evident that the range sidelobes are efficiently suppressed by about 38dB as we hoped and grating lobes are suppressed by about 35dB. We think we reach our goal to control the lobes by approximate weighting and improved parameter selection method to suppress grating lobes.

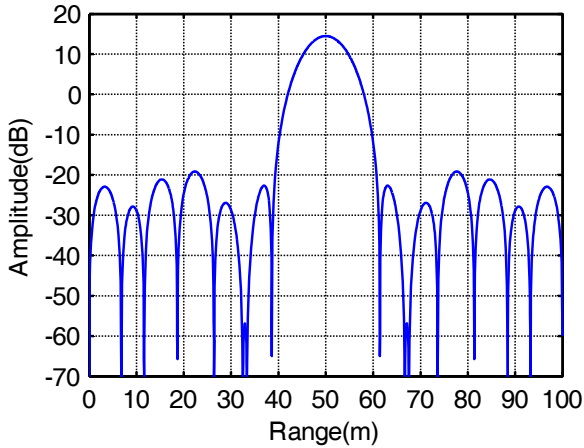


Fig.7 Range profile of a static point target by typical case 2

6 Doppler Effect

For a moving target with a uniform velocity, target motion will cause the Doppler effect. The Doppler effect impacts on the stepped frequency pulse train consists of two parts: (1) the effect on the sub-pulse compression, and (2) the step frequency part.

6.1 The Effect on the Sub-pulse Compression

Target motion will cause envelop drift after sub-pulse compression. Generally the signal processing of pulse compression is done in the range of -4dB of the main lobe. If the drift in IT_r is less than the half of range bin after pulse compression, the envelop variance is within the range of -4dB of the main lobe. Its effect is negligible. Specially:

$$|\Delta v| \leq \frac{c}{4IBT_r} \quad (19)$$

6.2 The Effect on the Step Frequency Part

Expand the phase of this part of the m^{th} pulse in (2):

$$\theta = 2\pi(\theta_i + \frac{2mT_r f_0}{c} v + \frac{2mi\Delta f T_r}{c} v + \frac{4Rf_0}{c^2} v + \frac{4iR\Delta f}{c^2} v) \quad (20)$$

where $\theta_i = \frac{-2(f_0 + i\Delta f)R}{c}$.

θ_i is a phase term independent of v and exerts no effect on range profile. The second term is linear phase term which leads to range walk and have almost no effect on the amplitude of the range profile. It will introduce range detection error. The third term is

quadratic phase term which causes non-uniform sample on frequency domain and results in distortion and cross-range spread of the range profile. The latter is so small that could be ignored. If we define range error less than half of the synthetic range bin and variance of quadratic phase in IT_r less than π as condition of the range profile we can obtain reasonable target's rang profile, we can obtain compensation requirement:

$$|\Delta v| \leq \frac{c}{4IT_r f_0} \quad (21)$$

$$|\Delta v| \leq \frac{c}{8I^2 \Delta f T_r} \quad (22)$$

Input the simulation parameters of typical case 2 from Eq. (19) into Eq. (21) and Eq. (22), we obtain $|\Delta v| \leq 2054$ m/s, $|\Delta v| \leq 2.05$ m/s and $|\Delta v| \leq 7.05$ m/s. So the Doppler effect impacts on the range profile of non-linear stepped-frequency pulse train is mainly on step frequency part. As f_0 and Δf increase, the requirement for accuracy of motion compensation increase significantly especially for Eq. (21).

7 Motion Compensation

Methods to estimate the target velocity and synthesize the range profile of stepped-frequency pulse train were recently discussed in [18-21]. Reference [18] has suggested a modified waveform with 64 pulses to be transmitted on each carrier. It need more time to obtain the range profile and the accuracy of estimation was affected by limited integration time of FFT. [19-21] proposed least bursts error, time-frequency compound approach and phase cancellation respectively to estimate the target velocity or synthesize the range profile. But they all need two bursts with different parameters to obtain a range profile.

7.1 Velocity Estimation

Under wideband conditions, the returns are the superposition of echo of multi-scatters of the target. Additionally there is different Doppler frequency on each frequency carrier. Traditional FFT can not be applied to the stepped-frequency pulse train. Denote the target length is ΔL which has W scatters each with Δr away. The signal could be written as:

$$y'(t) = \sum_{i=0}^{N-1} \sum_{m=q_{i-1}}^{q_i-1} \sum_{n=1}^W A_m \exp\left\{j2\pi\left[\frac{-2(f_0 + i\Delta f)(R + \Delta r_n)}{c} + \frac{2mT_r f_0 v}{c} + \frac{2mT_r i\Delta f v}{c}\right]\right\} \quad (23)$$

Through coherent integration, we obtain coarse estimation of target radial velocity \hat{v} . According to Cramer-Rao lower limit bound for target radial velocity of conventional pulse train and experimental data, we found this \hat{v} satisfy the compensation requirement of Eq. (22) even when SNR= -10dB on return signal. So by multiplication the phase term:

$$\theta' = \sum_{i=0}^{N-1} \sum_{m=q_{i-1}}^{q_i-1} \exp\left(-j2\pi i\Delta f \frac{2mT_r \hat{v}}{c}\right) \quad (24)$$

We can compensate the Doppler effect caused by quadratic phase term.

Now the pulse train could be considered as a train of same Doppler frequency. But between frequency carrier, θ_i will introduce an increment $\frac{2\Delta f R}{c}$. The signal could be written as:

$$y'(t) = \sum_{i=0}^{N-1} \sum_{m=q_{i-1}}^{q_i-1} \sum_{n=1}^W A_m \exp\left\{j2\pi\left[\frac{-2(f_0 + i\Delta f)(R + \Delta r_n)}{c} + \frac{2mT_r f_0 v}{c} + \frac{2mT_r i\Delta f \Delta v_{\Delta f}^{\wedge}}{c}\right]\right\} \quad (25)$$

where $\Delta v_{\Delta f}^{\wedge}$ is quadratic phase term compensation error introduced by Eq. (24).

On each frequency carrier, if the pulses are multiplied by the conjugate of the first pulse of their frequency carrier, we can nullify the increment introduced by Δf and affect of multi-scatters. But the coefficient of T_r delay between each frequency carrier becomes discontinuous. So we have to multiply the pulses on each frequency carrier except the first pulse by the last pulse of the pre-step frequency carrier serially to keep its continuity. After above processing, the amplitude of each pulse is also changed. Amplitude consistency is necessary before next processing. So the pulse train become:

$$y''(t) = \sum_{m=0}^{l-N-1} A_m \exp\left[j2\pi\left(\frac{2mT_r f_0 v}{c} + \frac{2mT_r i\Delta f \Delta v_{\Delta f}^{\wedge}}{c}\right)\right] \quad (26)$$

The variance of vestigial phase $\frac{2mT_r i\Delta f \Delta v_{\Delta f}^{\wedge}}{c}$ is from 0 to 0.024. So the pulse train could be considered as a long coherent conventional pulses train with the same frequency carrier and Doppler frequency. It will provide enhanced Doppler resolution. Applying FFT again to these pulses, we can obtain final estimation of \hat{v} .

7.2 Error Analyses

Velocity estimation by applying FFT to all pulses will result an error Δv_1 . Because of a long coherent time, Δv_1 is relatively small. Quadratic phase term compensation will introduce a vestigial phase $\frac{2mT_r i\Delta f \Delta v_{\Delta f}^{\wedge}}{c}$ which will cause a maxim frequency shift $\frac{2(l-N)T_r N\Delta f \Delta v_{\Delta f}^{\wedge}}{c}$. The maximum error it causes is:

$$\begin{aligned} \Delta v_2 &= \frac{2(l-N)T_r N\Delta f \Delta v_{\Delta f}^{\wedge}}{c} (l-N)T_r c / [2(l-N)T_r f_0] \\ &= \frac{(l-N)T_r N\Delta f \Delta v_{\Delta f}^{\wedge}}{f_0} \end{aligned} \quad (26)$$

Because f_0 on denominator is much larger than element, Δv_2 will be very small. So the total maximum target radial velocity estimation error is $\Delta v = \Delta v_1 + \Delta v_2$.

7.3 Cramer-Rao Lower Limit Bound

As returned signal is corrupted with white noise, we have limitation on the parameter estimation precision. The Cramer-Rao lower bound σ_v for velocity estimation of non-linear stepped-frequency pulse train is:

$$\sigma_v \geq \left[\frac{lc^2}{SNR16\pi^2 T e^2} \right]^{1/2} \quad (27)$$

where

$$Te^2 = \sum_{i=0}^{N-1} \sum_{m=q_{i-1}}^{q_i-1} (f_0 + i\Delta f)^2 \left[\frac{T_p^2}{12} + m^2 T_r^2 \right] - T_p \left[\sum_{i=1}^{N-1} \sum_{m=q_{i-1}}^{q_i-1} (f_0 + i\Delta f) m T_r \right]^2$$

Monte Carlo simulations were performed to verify the performance of Doppler matched filtering algorithm. Fig.8 displays the velocity Cramer-Rao bound as a function of SNR. The dashed line corresponds to the velocity standard deviation obtained via simulation of Doppler matched filtering algorithm. The solid line represents the Cramer-Rao bound. The number of Monte Carlo simulation was 1000. The x-coordinate represents the SNR before sub-pulse compression on return increasing in step of 5dB. After sub-pulse compression, the SNR improves $D = BT_p$ times, which was used in Cramer-Rao bound expression in Eq. (27). The experimental result from Doppler matched filtering algorithm closely matches velocity Cramer-Rao bound particularly for high SNR. Employ chirp sub-pulses with large time bandwidth product will obtain higher SNR after pulse compression and improve the accuracy of target velocity estimation.

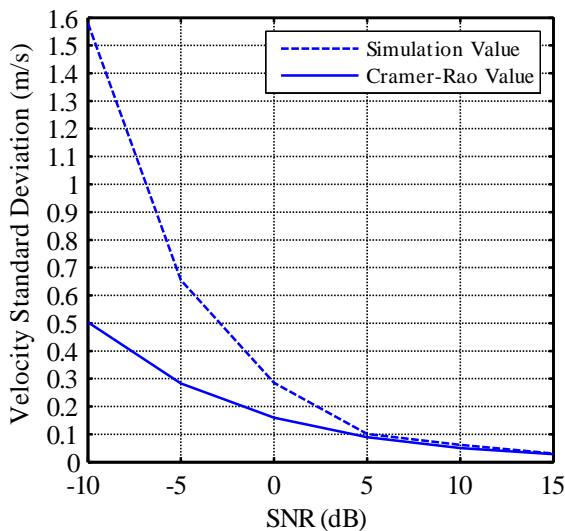


Fig.8 Simulation for velocity standard deviation and Cramer-Rao bound as a function of SNR

Fig.9 displays the effect of Δf to the accuracy of velocity estimation. The dashed line corresponds to the velocity standard deviation obtained via simulation of Doppler matched filtering algorithm for SNR=10dB. The solid line represents Cramer-Rao bound as a function of Δf .

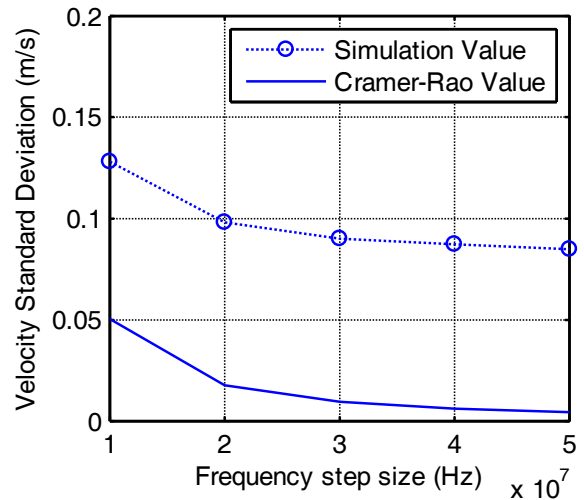


Fig.9 Simulation for velocity standard deviation and Cramer-Rao bound as a function of Δf for SNR=10dB

From Fig.9 we find that increase the frequency step size appropriately will also improve the accuracy of velocity estimation to a certain extent. Fig.10 shows the signal processing diagram of non-linear stepped-frequency pulse train.

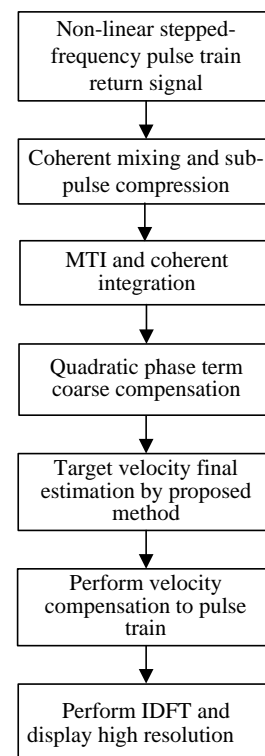


Fig.10 Flow chart of non-linear stepped-frequency chirp pulse train signal processing

7.4 Limitations

(1) FFT has its velocity measurement bound. It is still can be resolved by reducing T_r or using

diversity T_r on different frequency carrier to widen its measurement bound.

(2) Coherent integration could also resolve the targets of different radial velocity, so we can distinguish these targets. But there are few pulses on some frequency carriers which limits its resolution ability. More pulses are needed on these frequency carriers to improve its Doppler resolution ability.

(3) Compare to traditional stepped-frequency pulse train, this class of non-linear stepped-frequency transmits a great number of sub-pulses. It will need more time to obtain target one-dimensional range profile.

8 Conclusions

In this paper, we investigate a class of non-linear stepped-frequency chirp pulse train. By controlling the repetition number of each step frequency, we accomplish clutter cancellation and spectral weighting on transmitter and reach practically any desired sidelobes level. We discuss in detail in its grating lobes and relationship between parameters and present an improved approach to find parameters in a relatively wide range to form such pulse train with large $T_p \Delta f$, $T_p B$, small overlap ratio $B/\Delta f$ and small grating lobes. We provide several examples to prove its effectiveness. We also proposed a method to estimate target radial velocity in one burst. Closed-form expression of Cramer-Rao lower bound for velocity estimation is presented to demonstrate the performance of proposed method. The bound calculated from simulation was agreement with Cramer-Rao lower bound particularly in high SNR. Due to its efficiency and accuracy, it is found suitable to real-time processing. Additionally, this method is also applicable to similar train which has multiple sub-pulses on each frequency carrier.

Acknowledgments

This work is supported by the foundation of Arm in Advance (9140A07050806DZ0229)

References:

- [1] Wehner, D.R., *High-Resolution Radar (2nd edition)*, Artech House, Norwood, MA, USA, 1995.
- [2] Daniel, J.R., Nonlinear synthetic wideband waveforms, *Proceedings of IEEE Radar Conference*, 2002, pp. 212-219.
- [3] Lord, R.T., Inngs, M.R., High resolution SAR

processing using stepped-frequencies, *Proceedings of IEEE International Geoscience and Remote Sensing Symposium (IGARSS'97)*, vol.1, 1997, pp. 490-492.

- [4] Zhang, Q., Jin, Y.Q., Aspects of Radar Imaging Using Frequency-Stepped Chirp Signals, *Eurasip Journal on Advanced Signal Processing*, 2006, Doi: 10.1155/ASP/2006/85823.
- [5] Benjamin, C.F., Jae, S.S. and Salim, T., Efficient method for the translational motion compensation of inverse synthetic aperture radar imagery, *Optical Engineering*, Vol.40, No.3, 2001, pp. 433-442.
- [6] Levanon, N., Mozeson, E., Nullifying ACF grating lobes in stepped-frequency train of LFM pulses, *IEEE Transactions on Aerospace and Electronic Systems*, Vol.39, No.2, 2003, pp. 694-703.
- [7] Levanon, N., Stepped-frequency pulse-train radar signal, *IEE Proceedings of Radar, Sonar and Navigation*, Vol.149, No.6, 2002, pp. 297-309.
- [8] Chebanov, D., Low Sidelobe Nonlinear Stepped Frequency Waveforms, *SPIE Radar Sensor Technology XII, Orlando*, Vol.6947, 2008, pp. 69470H-1.
- [9] Keel, B.M., J.A. Saffold and M.R. Walbridge, Nonlinear stepped chirp waveforms with subpulse processing for range side lobe suppression, *Radar sensor technology III*, Orlando, FL, USA, Vol.3395, 1998, pp. 87-98.
- [10] Berens, P., SAR with ultra-high range resolution using synthetic bandwidth, *Proceedings of IEEE International Geoscience and Remote Sensing Symposium (IGARSS '99)*, vol. 3, 1999, pp. 1752-1754.
- [11] Bogard, J.N., D.H. Werner and P.L. Werner, Optimization of Peano-Gosper fractal arrays for broadband performance using genetic algorithms to eliminate grating lobes during scanning, *Antennas and Propagation Society International Symposium, 2005 IEEE*, Vol.1B, 2005, pp. 755-758.
- [12] Li, H.B, Y.H. Zhang and J. Wu, Sidelobes and grating lobes reduction of stepped-frequency chirp signal, *Microwave, Antenna, Propagation and EMC Technologies for Wireless Communications, 2005 (MAPE 2005)*, *IEEE International Symposium on Beijing*, Vol. 2, 2005, pp. 1210-1213
- [13] Lim, B.G. and Y.S. Kim, Simultaneous reduction of sidelobes and grating lobes by realising nonlinear synthetic wideband waveforms in SAR processing, *Electronics*

- Letters*, Vol. 44, No.24, 2008, pp. 1427-1428.
- [14] Dai, X.Z., J. Xu and Y.N. Peng, Suppressing HRRP grating lobes in stepped-frequency train of LFM pulses using extended correlation, *Electronics Letters*, Vol.43, No.25, 2007, pp. 1462-1466.
- [15] Long, H. and X.Z. Liu, Coherent synthesis sparse aperture radar with grating lobes suppressed using frequency MIMO technique, *Radar Conference, 2008. RADAR '08. IEEE*, pp. 1-5.
- [16] Maron, D.E., Frequency-jumped burst waveforms with stretch processing, *Radar Conference, 1990, Record of the IEEE 1990 International*, pp. 274-279.
- [17] Zhang, Q., Yeo, T. S. and Du, G., ISAR imaging in strong ground clutter using a new stepped-frequency signal format, *IEEE Transactions on Geoscience and Remote Sensing*, Vol.41, No.5, 2003, pp. 948-952.
- [18] Shen, Y.Y., Liu, Y.T., A step pulse train design for high resolution range imaging with Doppler resolution processing, *Chinese Journal of Electronics*, Vol.8, No.2, 1999, pp. 196-199.
- [19] Liu, Z. and Zhang, S.H., Estimation of target motion parameter in a stepped-frequency pulses radar, *ACTA Electronica Sinica*, Vol.28, No.3, 2000, pp. 43-45.
- [20] Wang, G.L., Li, X.G., Compound approach of measuring velocity based on step-frequency and pulse Doppler system, *Journal of Infrared Millimetre Waves*, Vol.27, No.3, 2008, pp. 190-192.
- [21] Chen, H.Y., Liu, Y.X., Jiang, W.D. and Guo, G.R., A new approach for synthesizing the range profile of moving targets via stepped-frequency waveforms, *IEEE Geoscience and Remote Sensing Letters*, Vol.3, No.3, 2006, pp. 406-409.